# Supporting Information

# A Wavy Two-Dimensional Covalent Organic Framework from Core-Twisted Polycyclic Aromatic Hydrocarbons

Marta Martínez-Abadía,[a] Craig T. Stoppiello,[b,c] Karol Strutynski,[d] Belén Lerma-Berlanga,[e] Carlos Martí-Gastaldo,[e] Akinori Saeki,[f] Manuel Melle-Franco,*[d] Andrei N. Khlobystov*[b,c] and Aurelio Mateo-Alonso*[a,g]

[a] *POLYMAT, University of the Basque Country UPV/EHU, Avenida de Tolosa 72, E-20018 Donostia-San Sebastian, Spain.*

[b] *School of Chemistry, University of Nottingham, University Park, Nottingham NG7 2RD, UK.*

[c] *The Nanoscale and Microscale Research Centre, University of Nottingham, University Park, Nottingham NG7 2RD, UK.*

[d] *CICECO - Aveiro Institute of Materials, Department of Chemistry, University of Aveiro, 3810-193 Aveiro, Portugal.*

[e] *Instituto de Ciencia Molecular, Universidad de Valencia, 46980 Paterna, Spain.*

[f] *Department of Applied Chemistry, Graduate School of Engineering, Osaka University, Suita, Osaka 565-0871, Japan.*

[g] *Ikerbasque, Basque Foundation for Science, Bilbao, Spain.*

**Table S1:** Crystal data and refinement for **HBC**.

| | |
|---|---|
| **Empirical formula** | $C_{48}H_{24}O_6$ |
| **Formula weight** | 696.67 |
| **Crystal system** | Triclinic |
| **Space group** | P-1 |
| **CCDC reference** | 1885013 |
| **a (Å)** | 13.0079(6) |
| **b (Å)** | 14.5518(5) |
| **c (Å)** | 18.7581(7) |
| **α (°)** | 67.779(4) |
| **β (°)** | 76.113(4) |
| **γ (°)** | 79.561(3) |
| **V (Å$^3$)** | 3174.7(2) |
| **Z** | 2 |
| **d (calculated) (g/cm$^3$)** | 0.729 |
| **μ (mm$^{-1}$)** | 0.388 |
| **F (000)** | 720.0 |
| **h** | -9 ≤ h ≤15 |
| **k** | -16 ≤ k ≤17 |
| **l** | -22 ≤ l ≤22 |
| **collected reflections** | 24416 |
| **independent reflections** | 11965 |
| **$R_{int}$** | 0.0291 |
| **GOF in $F^2$** | 1.033 |
| **$R_1$ [I>2σ(I)]** | 0.0784 |
| **wR($F^2$ ) [I>2σ(I)]** | 0.2489 |
| **$R_1$ (all data)** | 0.0989 |
| **wR($F^2$ ) (all data)** | 0.2681 |

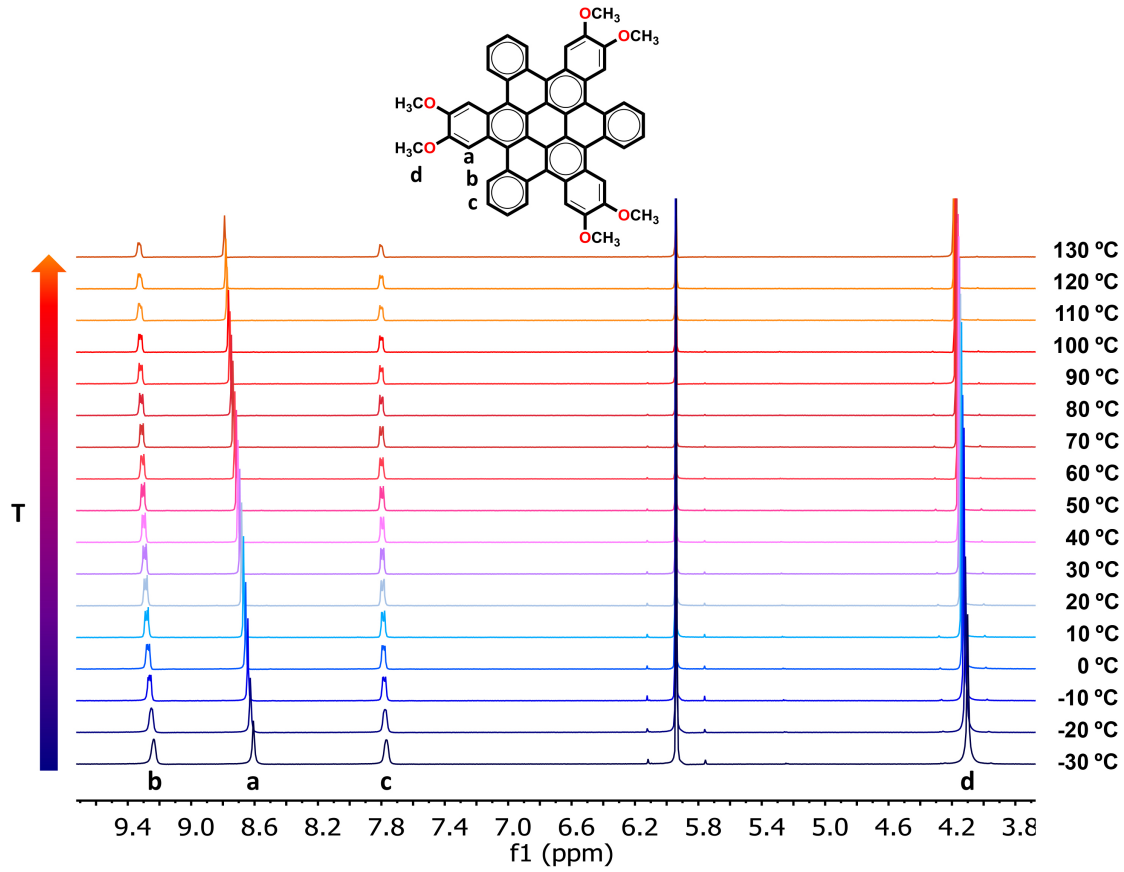


**Figure S1.** VT-NMR of 2,3,10,11,18,19-hexamethoxy-*cata*-hexabenzocoronene in 1,1,2,2-tetrachloroethane-$d_4$.

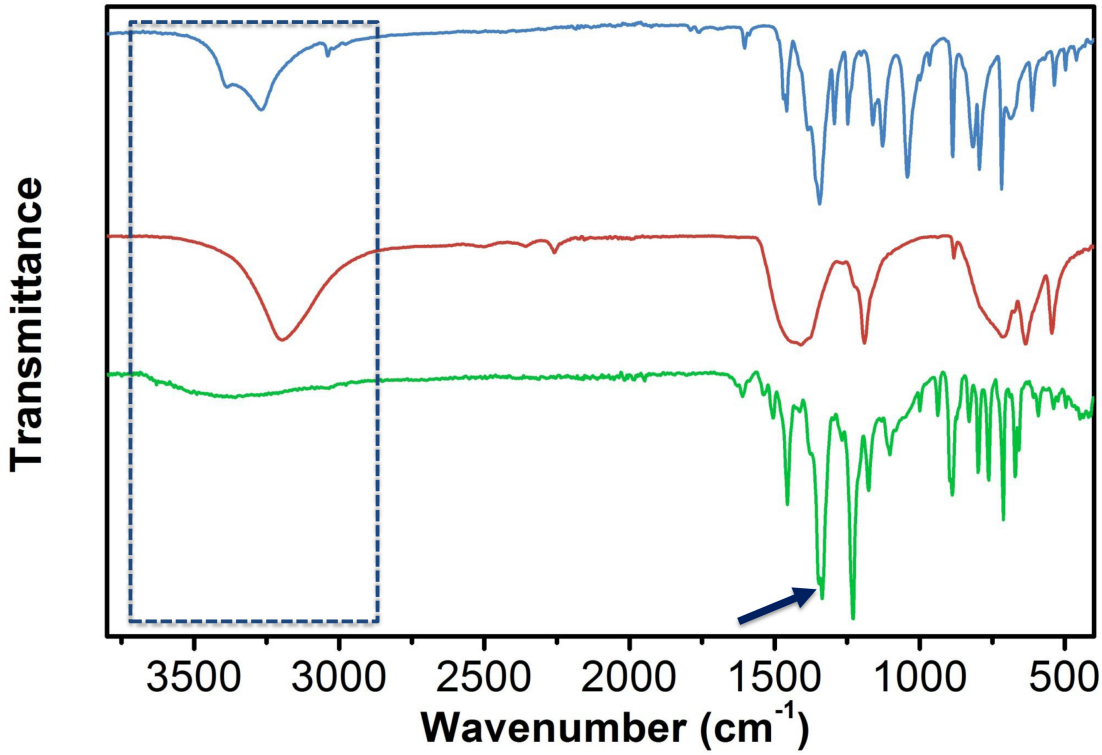


**Figure S2.** FTIR Spectra of **PDBA** (blue), **HBC** (red) and **Marta-COF-1** (green).

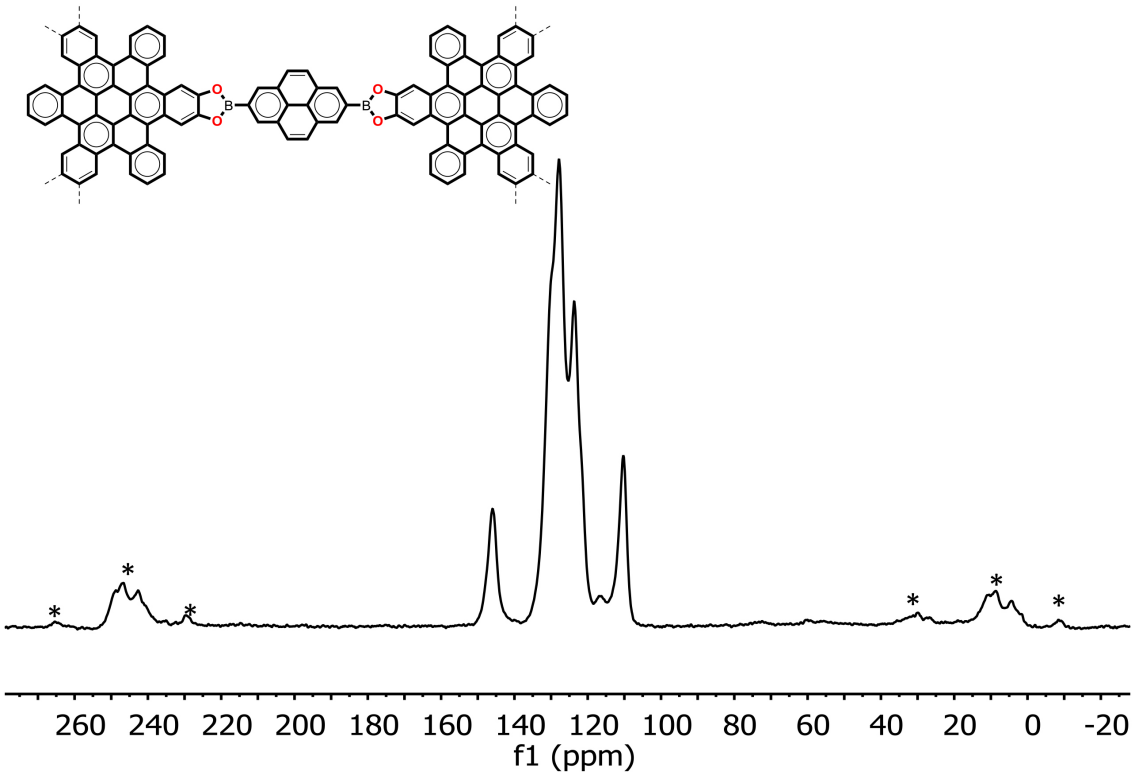


**Figure S3:** SS$^{13}$C NMR Spectrum of Marta-COF-1 (* indicate spinning side bands).

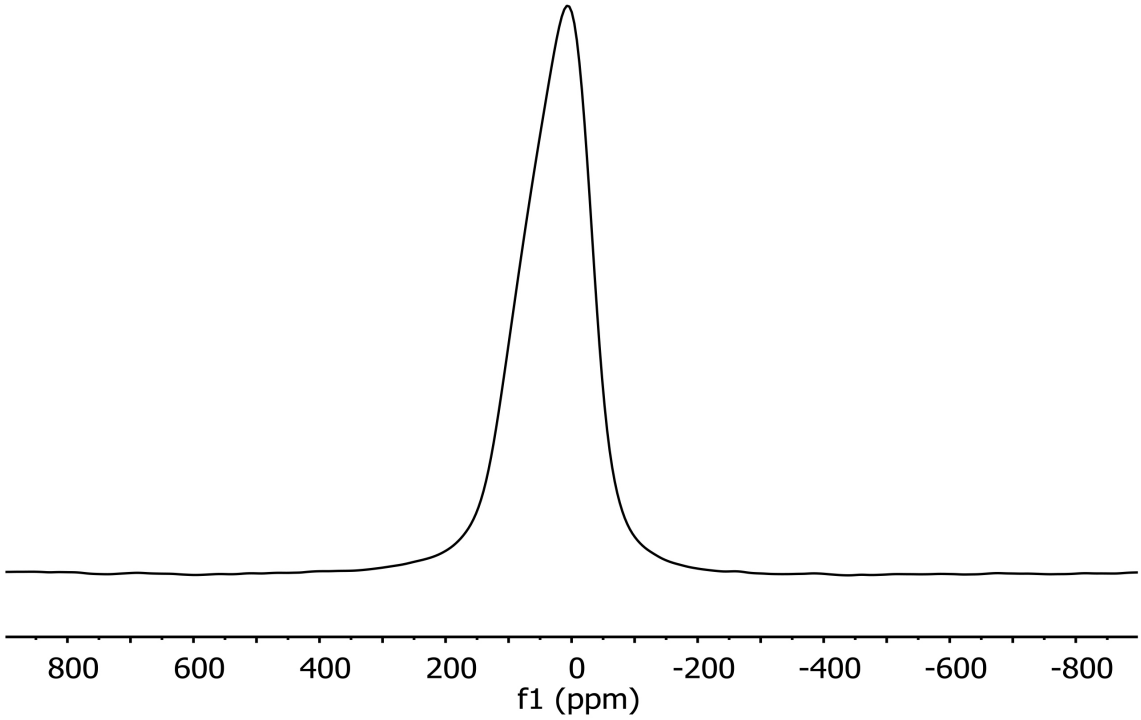


**Figure S4:** SS$^{11}$B NMR Spectrum of Marta-COF-1.

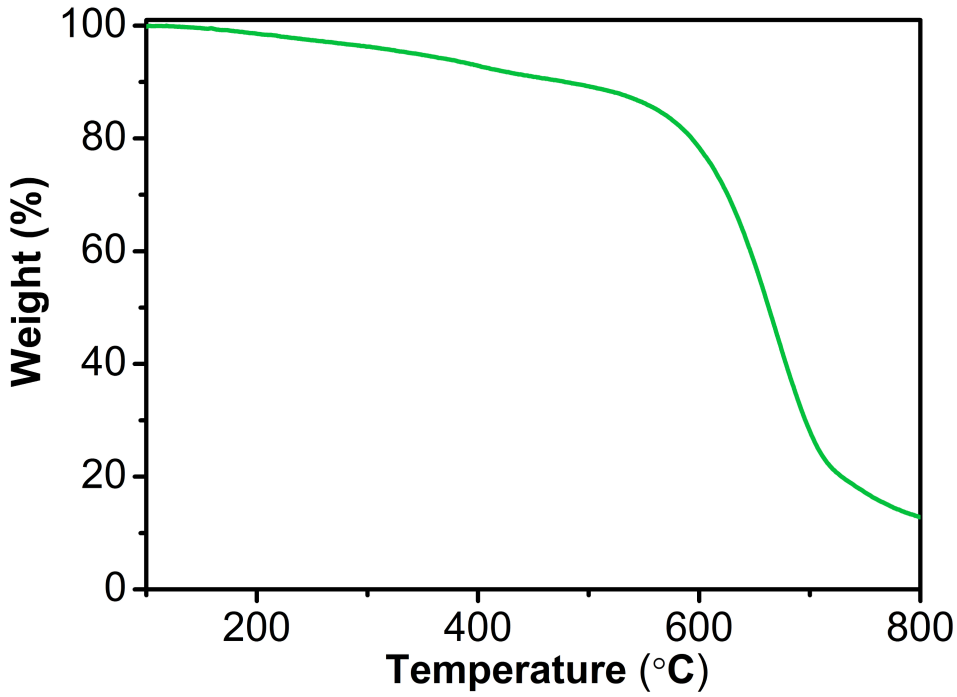


**Figure S5.** Thermogravimetric analysis of Marta-COF-1 performed at 10 ºC $min^{-1}$ under $N_2$ (air was flushed after 800 ºC).

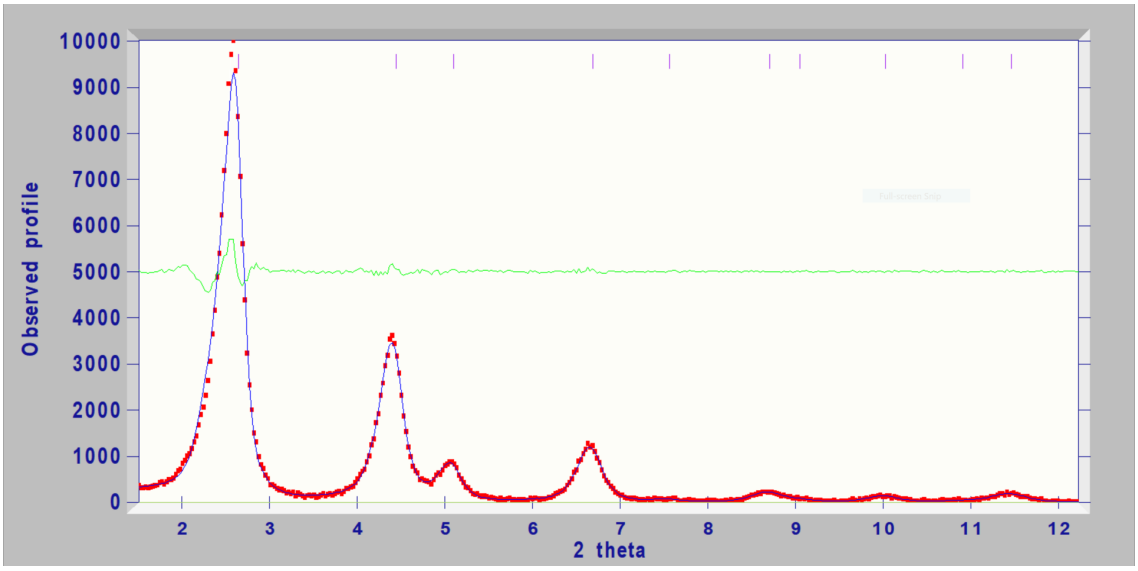


**Figure S6.** PXRD analysis for Marta-COF-1 including the experimental diffraction pattern (blue line), Pawley refined pattern (red dashed line), and the difference between the refined and experimental pattern (green line).

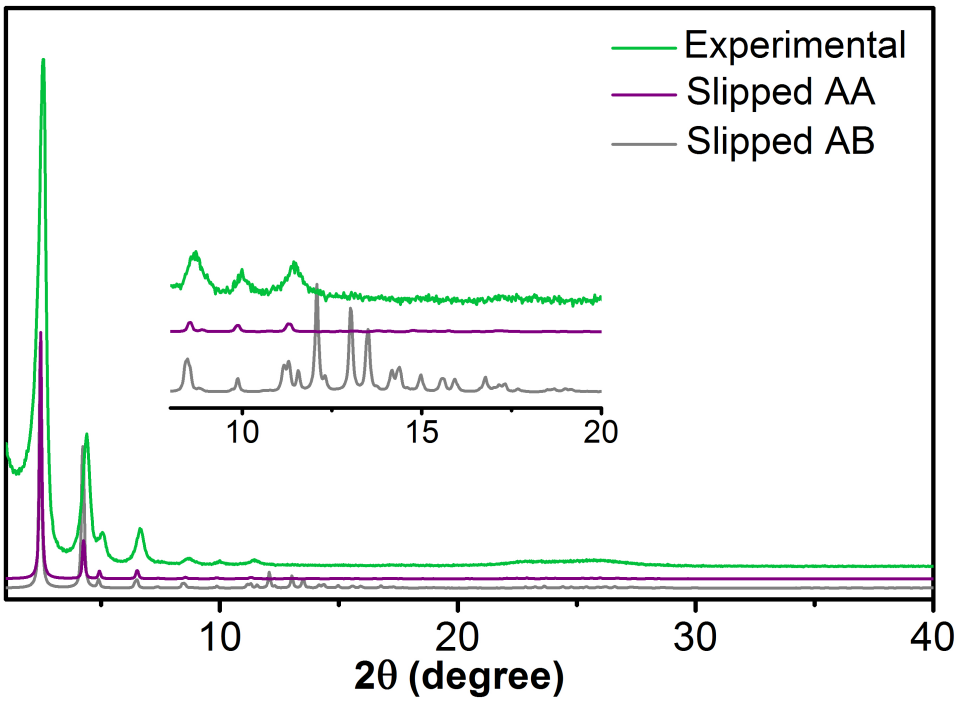


**Figure S7.** PXRD for Marta-COF-1 including the experimental (green line), the simulated slipped AA packing (purple) and the simulated slipped AB packing (gray) diffraction patterns.

**Table S2:** Binding energies (BE), frontier orbitals and gap obtained from DFT calculations.

| | BE (kcal $mol^{-1}$) | BE per heavy atom (kcal $mol^{-1}$) | HOCO (eV) | LUCO (eV) | Gap (eV) |
|---|---|---|---|---|---|
| 1 layer | | | -5.678 | -2.479 | 3.198 |
| AA | -289.210 | -0.893 | -5.767 | -3.064 | 2.703 |
| AB | -138.333 | -0.427 | -5.929 | -3.151 | 2.779 |

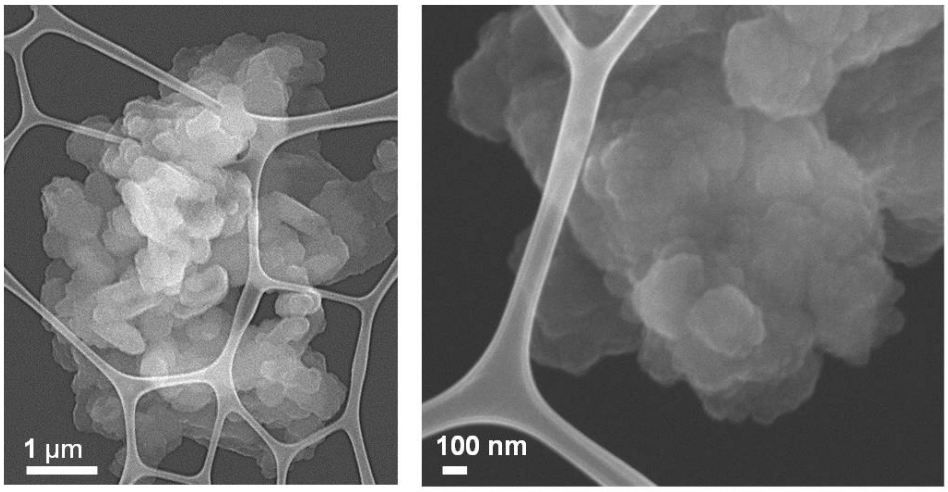


**Figure S8.** FE-SEM images of Marta-COF-1.

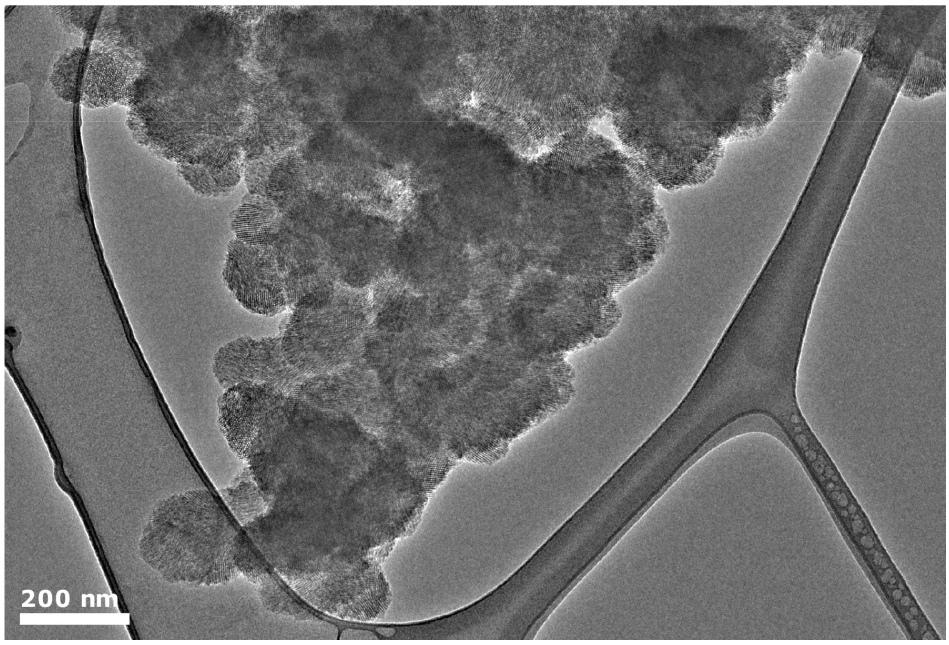


**Figure S9.** HR-TEM images of Marta-COF-1.

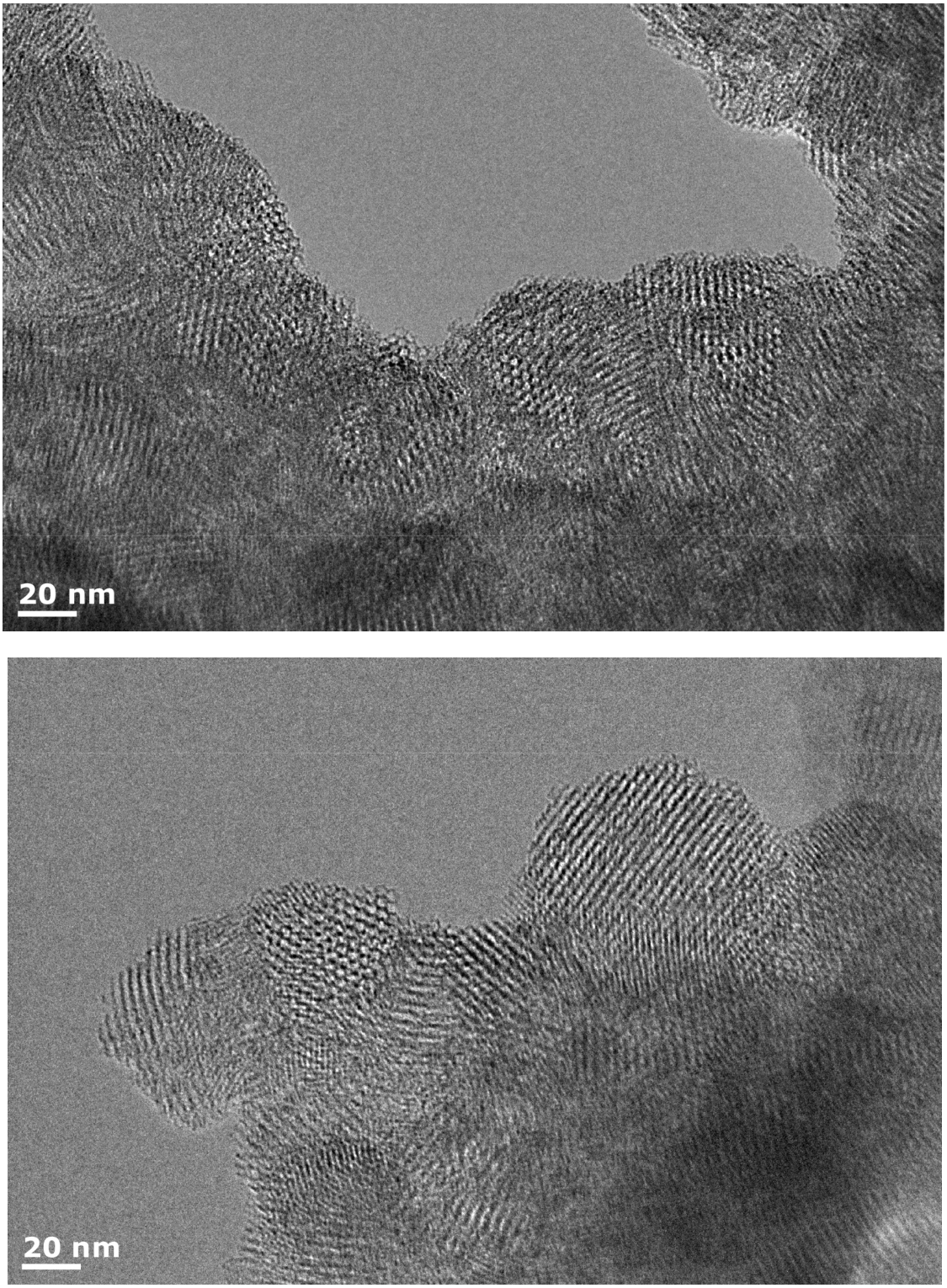


**Figure S10.** HR-TEM micrographs of Marta-COF-1 sitting face-on.

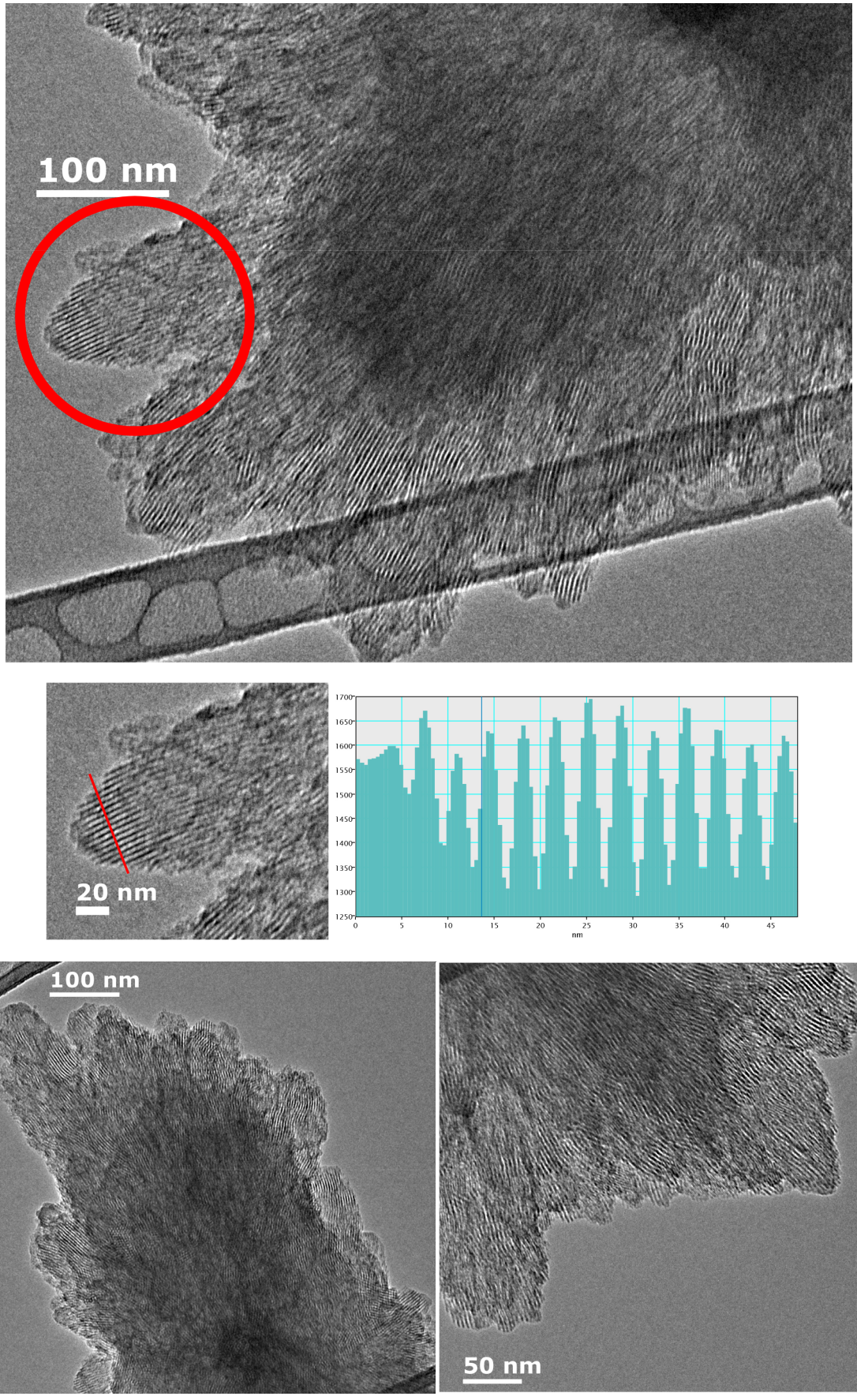


**Figure S11.** HR-TEM micrographs of Marta-COF-1 sitting edge-on, showing pore channels.

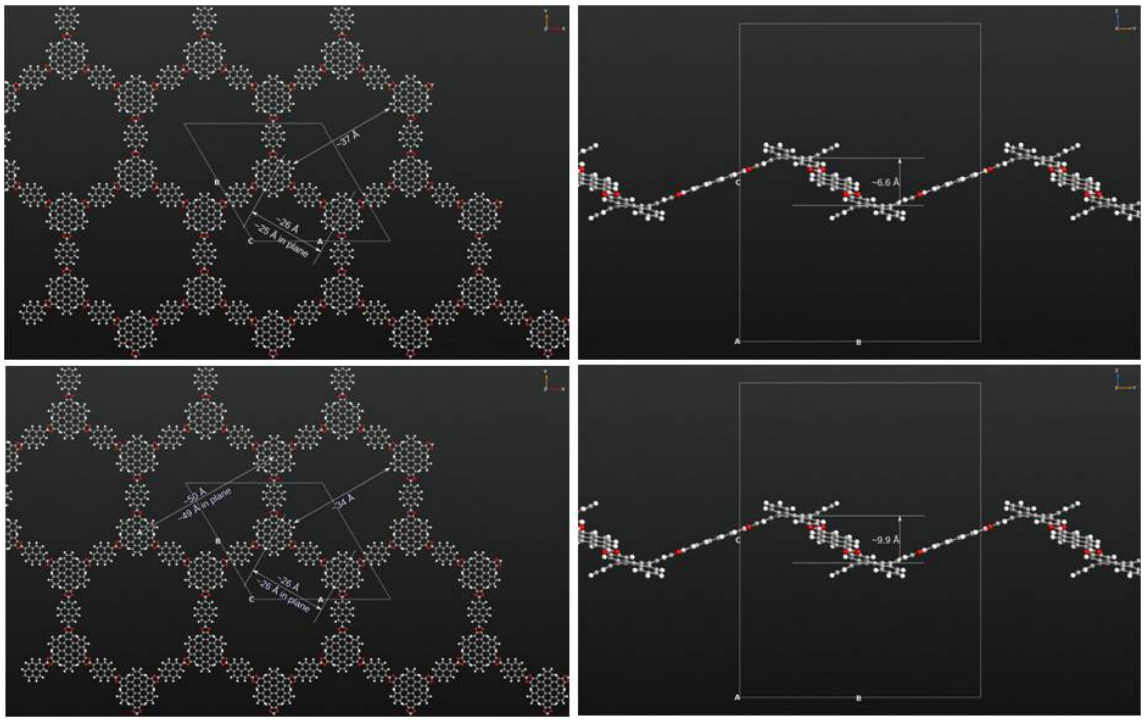


**Figure S12.** Structure of **Marta-COF-1**obtained from DFT. Single layer (top) and multi-layered (bottom) present slightly different arrangements. Each layer is undulated (right), but hexagonal pattern is preserved (left). The single layer exhibits a pore size slightly larger (3.7 nm) than the calculated for the multilayered (3.4 nm), and this is due to the packing produce a higher undulation (9.9 Å for the multi-layered *vs* 6.6 Å for a single layer).

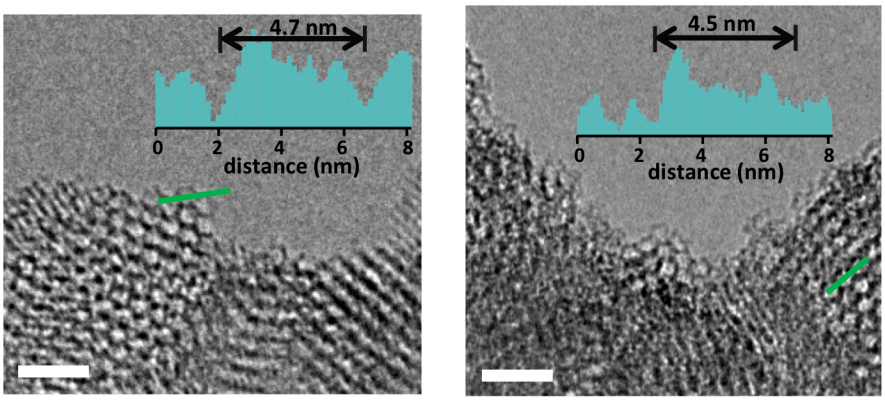


**Figure S13.** HR-TEM micrographs of **Marta-COF-1**. Inset of figures are line profiles from crystalline features (taken over the green lines) in both the edge (left) and the bulk of the structure (right) confirming the diameter decrease in the bulk of the domain. The scale bars are 10 nm.

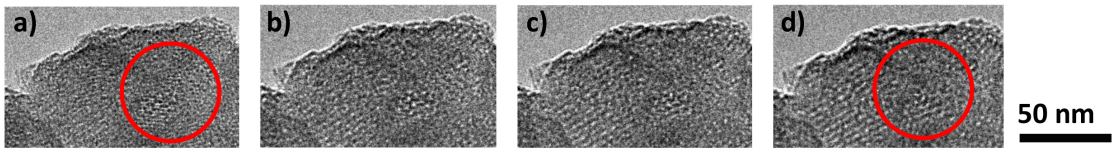


**Figure S14.** HR-TEM micrographs of **Marta-COF-1** where tilting part of the sample 25º leads to the observation of a chair-like configuration (d) from previously seen hexagons (a).

## Experimental procedures

Reagents for synthesis were, if not otherwise specified, purchased from Aldrich, TCI or Acros Organics. Column chromatography was carried out using Silica gel 60 (40-60 μm) from Scharlab. Analytical thin layer chromatography (TLC) was done using aluminum sheets (20x20 cm) pre-coated with silica gel RP-18W 60 F254 from Merck. UV-active compounds were detected with a UV-lamp from CAMAG at wavelength λ = 254 or 366 nm. Pyrene-2,7-diboronic acid (PDBA)[1] and 2,3,10,11,18,19-hexamethoxy-cata-hexabenzocoronene[2] were synthesized according to reported methods.

Marta-COF-1 was synthesized in a pre-scored 5 mL ampoule from Aldrich. For its synthesis and purification anhydrous 1,4-dioxane (99.8%), anhydrous acetone (99.8%), anhydrous hexane (97%) were purchased from Acros Organics. THF was dried using an Innovative Pure Solve solvent purification system and mesitylene (97%) was obtained from Acros Organics and dried with molecular sieves.

NMR spectra in solution were recorded on Bruker Avance 400 spectrometer at room temperature K using partially deuterated solvents as internal standards. Coupling constants (J) are denoted in Hz and chemical shifts (δ) in ppm. Multiplicities are denoted as follows: s = singlet, d = doublet, t = triplet, m = multiplet, br = broad.

Solid-State $^{1}H$, $^{11}B$ and $^{13}C$ CP/MAS NMR spectra were recorded on a Bruker Avance III 400 MHz NMR spectrometer at a MAS rate of 12 kHz and a CP contact time of 2 ms.

Matrix Assisted Laser Desorption Ionization (coupled to a Time-Of-Flight analyzer) experiments (MALDI-TOF) were recorded on Bruker REFLEX spectrometer in POLYMAT.

ATR-FTIR spectra were recorded on a Bruker ALPHA ATR-IR spectrometer.
TA Instruments Discovery system was used to perform the thermogravimetric analysis (TGA) using a 10 ºC $min^{-1}$ heating rate under a nitrogen flow, which was changed to oxygen from 800 ºC.

X-ray single crystal diffraction measurements were collected on an Agilent Technologies Super-Nova diffractometer, wich was equipped with monochromated Cu kα radiation (λ= 1.54184 Å) and Atlas CCD detector. Measurement was carried out at 150.00(10) K with the help of an Oxford Cryostream 700 PLUS temperature device. Data frames were processed (united cell determination, analytical absorption correction with face indexing, intensity data integration and correction for Lorentz and polarization effects) using the Crysalis software package. The structure was solved using Olex2 and refined by full-matrix least-squares with SHELXL-97. Final geometrical calculations were carried out with Mercury and PLATON as integrated in WinGX.

The powder X-ray diffraction (PXRD) patterns were collected by using a PHILIPS X'PERT PRO automatic diffractometer operating at 40 kV and 40 mA, in theta-theta configuration, secondary monochromator with Cu-Kα radiation (λ = 1.5418 Å) and a PIXcel solid state detector (active length in 2θ 3.347º). Data were collected from 1 to 50° 2θ (step size = 0.026 and time per step = 300 s, total time 40 min) at room temperature. A variable divergence slit, giving a constant 4.0 mm area of sample illumination, was used.

The pore structure was evaluated by nitrogen sorption isotherms, measured at 77 K with a Micromeritics 3Flex apparatus. The samples were degassed in an Autosorb station at and $10^{-6}$ Torr at 100 °C prior to analysis. Surface area, pore size and volume values were calculated from nitrogen adsorption-desorption isotherms (77 K). Specific surface area (SA) was calculated by multi-point Brunauer-Emmett-Teller (BET) method. Total pore volume was taken at $P/P_0$=0.96. Pore size distribution was analysed by using the solid density functional theory (NLDFT) for the adsorption branch by assuming a cylindrical pore model.

Electron Microscopy. All samples were prepared by dispersion in acetone and drop cast onto lacey carbon-coated copper TEM grids (Agar). High resolution SEM was performed on a JEOL 7100 F operated at 5 kV. High Resolution Transmission Electron Microscopy (HRTEM) analysis was performed on a JEOL2100F operating at 200 kV. The tilt series was taken using a Gatan 916 high tilt tomography holder, acquiring images at 1º tilt intervals and using a Gatan OneView electron detecting camera to ensure as low an electron dose as possible. The morphology of the samples was determined by taking low magnification (ca. x 30k mag) images from different regions of the specimen, and the nanoscale features were imaged using high resolution imaging (ca. x 100k mag).

FP-TRMC experiments were conducted for the sample on a quartz plate using the third harmonic generator (THG; 355 nm) of a Nd:YAG laser (Continuum Inc., Surelite II, 5–8 ns pulse duration, 10 Hz) as the excitation source ($9.1 \times 10^{15}$ photons $cm^{-2}$ $pulse^{-1}$). The frequency and power of microwave were ~9.1 GHz and 3 mW, respectively. The photoconductivity transient Δσ was converted to the product of the quantum yield ($\varphi$) and the sum of charge carrier mobilities $\sum\mu$ (= $\mu_+ + \mu_-$) by the formula $\varphi\sum\mu = \Delta\sigma(eI_0F_{light})^{-1}$, where $e$ and $F_{light}$ are the unit charge of a single electron and a correction (or filling) factor, respectively. Thin films were prepared as follows: Marta-COF-1 (0.2 mg) and PTAA (polytriarylamine, Aldrich 2.0 mg) were dispersed in toluene (1.1 mL). After stirring at 80 ºC for 1 h, the solution was spin-coated on a quartz substrate at 500rpm for 3 min. Then, the remaining solvent was completely removed in a vacuum chamber for 1 h. The sample thickness is ~ 110 nm.

## Synthesis and characterization

**HBC:** 2,3,10,11,18,19-hexamethoxy-cata-hexabenzocoronene (20 mg, 0.0256 mmol) was dissolved in dichloromethane (2 mL) and then $BBr_3$ (1M solution in dichloromethane) was added (2 mL) at 0 ºC. The suspension was stirred overnight at room temperature. The solvents were removed with a nitrogen flow and the solid was washed with dichloromethane. After that, methanol was added (8 mL) and removed again with a nitrogen flow. Finally, the solid was dried under vacuum (quantitative yield).
$^1$H NMR (400 MHz, $(CD_3)_2CO$): δ 9.32 – 9.24 (m, 6H), 8.74 (s, 6H), 7.89 – 7.81 (m, 6H). $^{13}$C NMR (101 MHz, $(CD_3)_2CO$): δ 147.00, 131.16, 129.66, 127.40, 126.23, 125.69, 121.45, 114.06. EM (MALDI-TOF) (m/z): calculated for $C_{48}H_{24}O_6$: 696.157; found: 696.164 $[M]^+$.

**Marta-COF-1:** HBC(13.67 mg, 0.0196 mmol) and pyrene-2,7-diboronic acid (8.50 mg, 0.0293 mmol) were sonicated in 2 mL of a mixture of degassed 1,4-dioxane/mesitylene (2:1) in a pre-scored 5 mL ampoule under nitrogen. The suspension was degassed by using three freeze-pump-thaw cycles. The ampoule was sealed off using flame and heated at 125 ºC for 3 days.The yellow precipitate was collected by filtration and washed five times with anhydrous tetrahydrofurane, acetone and hexane. The powder was dried at 30 ºC under vacuum for 24 hours. 19 mg of Marta-COF-1 was obtained (95 % yield).
SS$^1$H-NMR (δ) (ppm): 7.31. SS$^{13}$C-NMR (δ) (ppm): 145.9, 129.9, 127.9, 123.7, 121.7, 116.6, 110.3. ATR-FTIR ($cm^{-1}$): 1456, 1347, 1337, 1230.

## NMR spectra of HBC

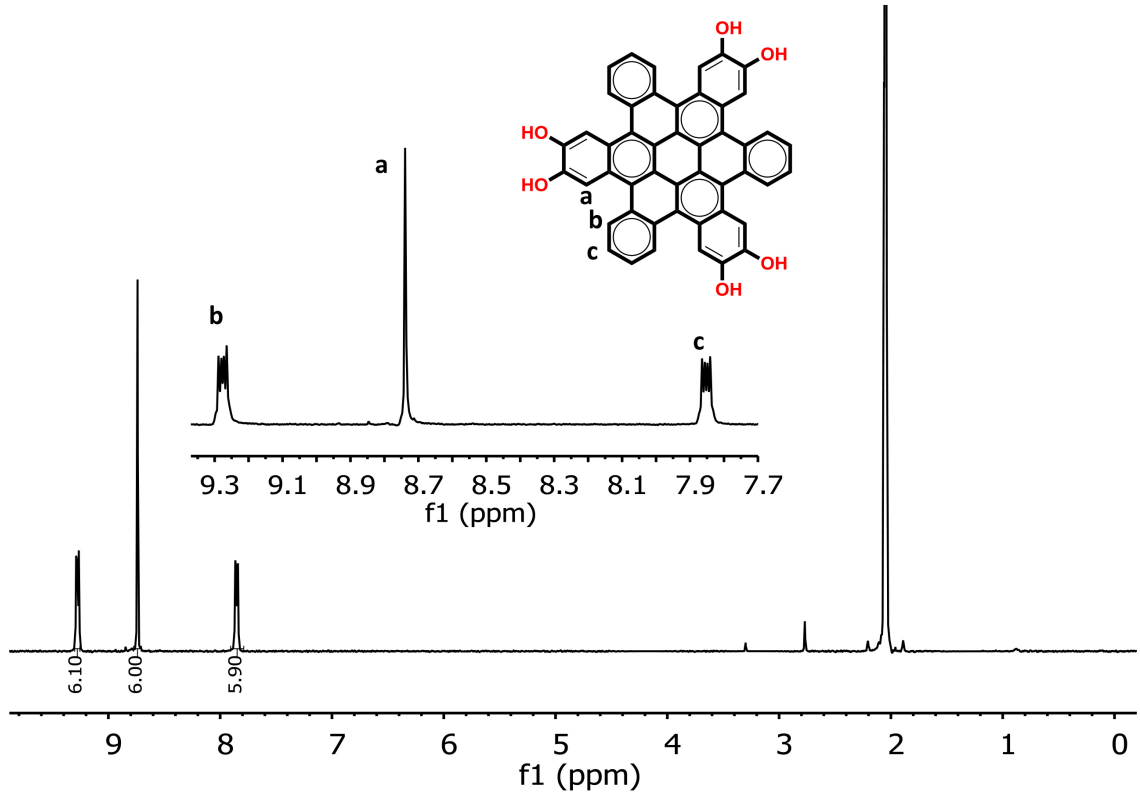


**Figure S15.** $^{1}$H NMR spectrum of HBC (400 MHz, $(CD_3)_2CO$, 298 K).

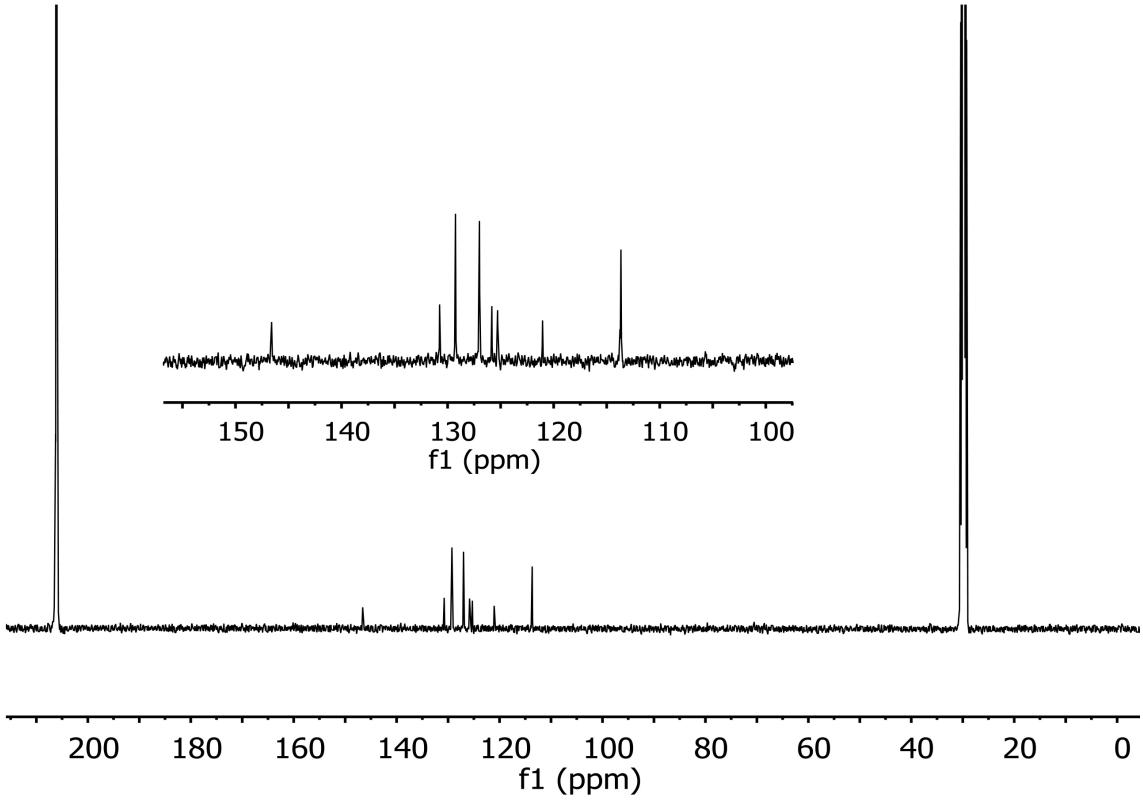


**Figure S16.** $^{13}$C NMR spectrum of HBC (100 MHz, $(CD_3)_2CO$, 298 K).

**Modelling and predicting electronic properties**

Two methods were applied to study the structure and electronic properties of Marta-COF-1: Density Functional Theory (DFT) and semi-empirical Density Functional Theory Tight Binding (DFTB). Both are based on the LCAO approximation but differ in the computational resources required, as the DFT method requires considerably more resources but it is also more accurate. Marta-COF-1 has a direct band gap in the $\Gamma$-point and this was the only point used in the calculations. The PBE functional was chosen for the geometry optimizations due to its transferability and the fact that it's more affordable computationally than hybrid functionals. In order to include dispersion interactions, the so-called range-separated MBD@rsSCS was employed. Band gaps were computed with the B3LYP functional (with Tkatchenko-Scheffler vdW corrections). All DFT calculations were done using the Fritz Haber Institute ab initio molecular simulations (FHI-aims) package[3-5] using "light" numeric atomic orbitals, which approximately correspond to a TZVP gaussian basis set.
Tight binding calculations were done using the "matsci" parameter set with DFTB+ program[6] with Lennard-Jones dispersion corrections.

Different interlayer stackings, namely: AA and AB structures were tried. These stackings differ in the relative location of the layers. In AA, the second layer is directly on top of the first one while in AB, the second layer is shifted by half of the hexagon height.

All investigated conformations were pre-optimized using DFTB while final optimizations were performed using DFT for AA and AB. To elucidate the most stable stacking thermodynamically, the energy of the different conformations was compared. Tables S2 and S3 summarize the results obtained from the DFT calculations, unit cell parameters, atoms in unit cell, binding energies (BE, frontier orbitals and corresponding electronic gaps. Note that both methods, DFT and DFTB (not shown here), predict AA to be the most thermodynamically stable stacking. According to tight binding, ABC's binding energy is between AA and AB stackings.

**Table S3:** Unit cell parameters obtained from DFT calculations.

| | Atoms per unit cell | Heavy atoms per unit cell | a (Å) | b (Å) | c (Å) | alpha | beta | gamma |
|---|---|---|---|---|---|---|---|---|
| 1 layer | 222 | 162 | 43.74 | 43.68 | 50.10 | 90.00 | 90.00 | 120.00 |
| AA | 444 | 324 | 41.18 | 41.62 | 8.10 | 90.00 | 90.00 | 120.00 |
| AB | 444 | 324 | 41.47 | 42.03 | 7.83 | 90.00 | 90.00 | 120.00 |

Interestingly, in the structures optimized using DFT, nodes are not directly on top of each other but are shifted slightly in a graphite-like interlayer pattern (Figure S17).

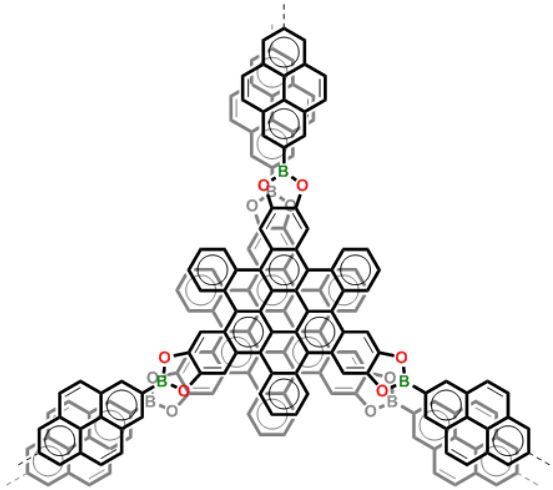

**Figure S17.** Graphite-like structure between the nodes predicted by Density Functional Theory.

## References


1. G., C. A.; Zhiqiang, L.; I., M. I. A.; Marie-Hélène, T.; Nicolle, S.; Gilles, A.; Andreas, S.; C., C. J.; S., B. A.; K., H. J. A.; B., M. T., Synthesis of 2- and 2,7-Functionalized Pyrene Derivatives: An Application of Selective C□H Borylation. *Chem. -Eur. J.* **2012,** *18* (16), 5022-5035.
2. Zhang, Q.; Peng, H.; Zhang, G.; Lu, Q.; Chang, J.; Dong, Y.; Shi, X.; Wei, J., Facile Bottom-Up Synthesis of Coronene-based 3-Fold Symmetrical and Highly Substituted Nanographenes from Simple Aromatics. *J. Am. Chem. Soc.* **2014,** *136* (13), 5057-5064.
3. Blum, V.; Gehrke, R.; Hanke, F.; Havu, P.; Havu, V.; Ren, X.; Reuter, K.; Scheffler, M., Ab initio molecular simulations with numeric atom-centered orbitals. *Comput. Phys. Commun.* **2009,** *180* (11), 2175-2196.
4. Marek, A.; Blum, V.; Johanni, R.; Havu, V.; Lang, B.; Auckenthaler, T.; Heinecke, A.; Bungartz, H. J.; Lederer, H., The ELPA library: scalable parallel eigenvalue solutions for electronic structure theory and computational science. *J. Phys. Condens. Matter* **2014,** *26* (21), 213201.
5. Yu, V. W.-z.; Corsetti, F.; García, A.; Huhn, W. P.; Jacquelin, M.; Jia, W.; Lange, B.; Lin, L.; Lu, J.; Mi, W.; Seifitokaldani, A.; Vázquez-Mayagoitia, Á.; Yang, C.; Yang, H.; Blum, V., ELSI: A unified software interface for Kohn–Sham electronic structure solvers. *Comput. Phys. Commun.* **2018,** *222*, 267-285.
6. Aradi, B.; Hourahine, B.; Frauenheim, T., DFTB+, a Sparse Matrix-Based Implementation of the DFTB Method. *J. Phys. Chem. A* **2007,** *111* (26), 5678-5684.